Monthly Notices
of the
ROYAL ASTRONOMICAL SOCIETY

Mon. Not. R. Astron. Soc. **400,** 875–886 (2009) doi:10.1111/j.1365-2966.2009.15493.x

A lensing view on the Fundamental Plane

Dominik Leier[1,2]★

[1]*Institute for Theoretical Physics, University of Zürich, Winterthurerstrasse 190, 8057 Zürich, Switzerland*
[2]*Astronomisches Rechen-Institut, Zentrum für Astronomie der Universität Heidelberg, Mönchhofstrasse 12-14, 69120 Heidelberg, Germany*

Accepted 2009 August 4. Received 2009 August 4; in original form 2009 March 29

ABSTRACT

For lensing galaxies, we introduce a formal velocity dispersion $\sigma_{\rm lens}$, based on enclosed mass and the virial theorem. This is calculated from an ensemble of pixelated lens models, and found to be fairly model-independent. A sample of 18 well-known early-type lensing galaxies and two clusters is found to be consistent with $\sigma_{\rm lens} = \sigma_{\rm obs}$. Both the early-type lensing galaxies and the clusters can thus be determined as being virialized. In a second step, we calculate the *I*-band luminosity and the total mass content for the sample of lensing galaxies, which enables us to analyse the mass-to-light relation $L \propto M^{\alpha}$. We determine $\alpha = 0.70 \pm 0.08$, excluding constant M/L and consistent with previous studies of the Fundamental Plane. Additionally, we verify that this relation does not extrapolate to clusters, which have a much higher M/L. The sample used for this analysis comprises nine lensing galaxies from the Sloan Lens ACS (Advanced Camera for Surveys) Survey and another nine from the CfA-Arizona Space Telescope LEns Survey as well as the lensing clusters ACO 1689 and ACO 2667.

Key words: gravitational lensing – galaxies: clusters: general – galaxies: elliptical and lenticular, cD – galaxies: fundamental parameters.

1 INTRODUCTION

The Fundamental Plane (FP) for early-type galaxies is a well-known scaling relation between the effective radius $R_{\rm eff}$, the kinematic velocity dispersion $\sigma_{\rm obs}$ and the surface brightness $I_{<R_{\rm eff}}$ (Djorgovski & Davis 1987; Dressler et al. 1987). Not so well understood is the mismatch between theoretical predictions for the FP on the one hand and observations on the other. Combining the virial theorem

$$M \propto R_{\rm eff}\sigma^2 \tag{1}$$

and the universality of light profiles $L \propto R_{\rm eff}^2 I$ while assuming a constant mass-to-light ratio yields

$$R_{\rm eff} \propto \sigma^2 I^{-1}, \tag{2}$$

which we name as the Vanilla Plane. In contrast, observations show a relation with slightly different power indices *a* and *b*, as in

$$R_{\rm eff} \propto \sigma^a I^b, \tag{3}$$

with $a \approx 1.2$ and $b \approx -0.8$ (e.g. Jørgensen, Franx & Kjaergaard 1996). The power indices are thus not in agreement with the Vanilla Plane indices $(a, b) = (2, -1)$ for constant M/L, which is suggestive of an underlying regularity beyond the above formulae.

With gravitational lensing as an independent measure of mass, one can suitably analyse the structure of the FP as already done in different approaches. Bolton et al. (2007) linked lensing mass and virial mass, whereas Rusin, Kochanek & Keeton (2003a), Treu et al. (2006), Jiang & Kochanek (2007, hereafter JK07) and Ferreras, Saha & Burles (2008) analysed the mass-to-light dependence

$$M^{\alpha} \propto L, \tag{4}$$

which is a representation of the FP.

By repeating the step from equations (1) to (2) for the more general definition of the mass-to-light relation in equation (4), *a* and *b* in equation (3) can be expressed in terms of the power index α, which is what we need to compare the results with previous FP-type studies (listed in Table B2). Equating the now α-dependent exponents of σ and *I* yields

$$a(b) = -2(1 + 2b), \tag{5}$$

which only applies for a mapping from (a, b) to α assuming equation (4). In other respects this mapping is not unique since different α values for *a* and *b* respectively may exist.

In this study, we combine both the virial approach and considerations including luminosities by means of lensing masses $M_{\rm lens}$ from 18 early-type lensing galaxies and two clusters discussed in detail in Section 2.

An important role is played by a formal velocity dispersion, which we define as

$$\sigma_{\rm lens}(R) = \sqrt{\frac{2}{3}\frac{GM(<R)}{\pi R}}. \tag{6}$$

For an isothermal sphere, this is exactly equal to a line-of-sight velocity dispersion. A short introduction to the determination of $\sigma_{\rm lens}(R)$ with the mass reconstruction method PIXELENS and a detailed description of the lensing sample (see Table B1) will be presented in

★E-mail: leier@physik.uzh.ch

Section 2. We define $M_{\rm lens}$ and $M_{\rm vir}$ by comparison with equation (1) as

$$M_{\rm lens} = \frac{3\pi}{2G} R_{\rm eff} \sigma^2_{\rm lens} \tag{7}$$

and $M_{\rm vir} = \frac{3\pi}{2G} R_{\rm eff} \sigma^2_{\rm obs}$.

This in hand we consider the following questions as a rephrased puzzle of FP.

(1) Is the lensing-inferred velocity dispersion $\sigma_{\rm lens}$ from non-parametric mass reconstruction equal to the kinematic velocity dispersion $\sigma_{\rm obs}$?
(2) Is this applicable to cluster scale-lensing objects?
(3) Are the computed $M_{\rm lens}$ and $M_{\rm vir}$ consistent with the FP?
(4) Does the FP relation extend to clusters?

Bearing this in mind, we want to give a short overview of previous findings.

In the above-mentioned approach by Bolton et al. (2007) to the FP problem, they find that $\sigma_{\rm lens} \approx \sigma_{\rm obs}$ without taking advantage of luminosities (see also Bolton et al. 2008). This result is comparable to the findings presented in Section 3 of this paper. Furthermore, Bolton et al. (2007) take no baryonic information into account, but a different plane is introduced, which emerges from a dimensional change in the FP space from surface brightness I to surface density Σ, giving

$$R_{\rm eff} \propto \sigma^{a_m} \Sigma^{b_m}.$$

But in fact this scaling relation, named a more fundamental or mass plane (MP), can be transformed into the shape $M^{-b_m}/R_{\rm eff}^{-(1+2b_m)} \propto \sigma^{a_m}$ which is consistent with our theoretical assumptions of equation (6) and thus represents the virial theorem. We would like to point out that the change to Σ introduces basically a redshift dependence, which comes along with a grave selection effect that reduces the significance of the scaling relation. Moreover, this relation is compared to the existing FP by introducing a new parametrization of the lensing mass

$$M_L = c \left[G^{-1} \sigma^2_{\rm obs} (R_{\rm eff}/2) \right]^{\delta},$$

where c denotes a structure constant and δ denotes a newly introduced power index. Bolton et al. (2007) find that by doing so 'the tilt relative to the virial relation is essentially eliminated'. But, basically c and δ are again consistent with equation (6). Upon choosing $\delta = 1$, c becomes $\log 3\pi/2$ and the new parametrization in Bolton et al. (2007) turns into a test of the virial theorem.

Thus, the decreased scatter for an MP is rather a natural consequence of the added fitting parameter and selection effects than a more fundamental scaling relation. Implications on structure variations are hardly possible. An appropriate treatment on the search for reasons for a tilt in the FP originating in certain structural peculiarities includes more elaborate approaches that allow for a distinction between for instance anisotropy and mass-dynamical structure.

Rusin et al. (2003a) introduced a self-similar mass model for early-type galaxies, consisting of two components: a concentrated component, which traces the light distribution, and a more extended power-law component, which represents the dark matter. They found a strong r^{-2} dominance, and therefore used the velocity dispersion $\sigma_{\rm iso}$ for an isothermal model as a surrogate in the FP yielding a mass-to-light relation of $M_{\rm lens}^{0.88^{+0.10}_{-0.11}} \propto L$, which was the first such result from strong lensing. The error of the slope already excluded a constant M/L. While substituting $\sigma_{\rm iso}$ they are effectively assuming the virial theorem.

JK07 constrain the average stellar mass fraction of a halo in favour of adiabatically compressed halo models by taking a sample of early-type galaxies which consists partially of lensing galaxies used in this sample. By means of a two-component model, stellar and virial masses are fitted separately and an isothermal density profile is assumed. This paper takes advantage of already K-corrected B-band magnitudes and lensing masses and is, because of its common subset of gravitational lenses, directly comparable with our data. Although it is not explicitly calculated in their paper, by taking their data we found $M_{\rm lens}^{0.88\pm0.12} \propto L$, which is in perfect agreement with the result from Rusin et al. (2003a).

Switching from the lensing point of view considering $M_{\rm lens}$ to the observational one considering $M_{\rm vir}$ enables one to compare the FP from previous studies which were inferred from lensing with the FP based on stellar dynamics. Treu et al. (2006) analyse the FP by means of virial mass and find that the velocity dispersions for their Sloan Digital Sky Survey (SDSS) lens sample are well approximated by $\sigma_{\rm iso}$, which holds also for our mixed CfA-Arizona Space Telescope LEns Survey (CASTLES)/Sloan Lens ACS (Advanced Camera for Surveys) Survey (SLACS) sample.

There are studies, for example from Graham & Colless (1997) and Trujillo, Burkert & Bell (2004), which raised hope that a solution for the FP tilt is at least partially given by broken structural homology leading to strong correlations between Sérsic index n and photometric-independent galaxy properties. Graham & Colless (1997) fit $R^{1/n}$ profiles and make use of the spatial velocity dispersion at spatial effective radius to show the influence of structural non-homology, whereas Trujillo et al. (2004) quantify the contribution to the tilt caused by variations of n for a wide range of B-band-selected early-type galaxies. The results always show that taking account of non-homology shifts the FP parameters closer but never fully matches the virial expectations. However, by comparing the M/L– σ relation of 25 E/S0 galaxies from the SAURON sample with the predictions and virial estimates, Cappellari et al. (2006) find that the FP tilt is exclusively due to a real M/L variation, while structural and orbital non-homology has a negligible effect, a result also verified in this study.

Furthermore, progress in estimating $M_{\rm tot}/M_{\rm stel}$ was recently made by comparing stellar population models with the non-parametric mass profiles also used in this paper, which allow for scanning the dark matter distribution within a galaxy (Ferreras, Saha & Williams 2005; Ferreras et al. 2008). They found that low-mass galaxies have only little dark matter content at all observed radii. On the contrary, high-mass galaxies have little or no dark matter inside the effective radius but at large radii they are clearly dark matter dominated. No kinematic and virial assumptions were required.

In this paper, we are using combination of kinematic, photometric and lensing-inferred data to answer the aforementioned puzzle. The comparison of $\sigma_{\rm obs}$ and $\sigma_{\rm lens}$, which is proportional to a comparison between virial mass and lens mass, is adequate for answering the above questions 1 and 2 as will be shown in Section 3. In Section 4, we compute the luminosities of the lenses, $M_{\rm lens}$ and $M_{\rm vir}$, needed for $L \propto M^{\alpha}$ and check the consistency with other FP studies in particular with data from JK07, who use a common subset of lens systems. Subsequently, the a-b-parameter plane is generated including a wide range of recent FP studies. In Section 5, the conclusions are presented.

2 LENSES AND LENS MODELS

In this section, we introduce the lensing sample and subsequently discuss the lens modelling.

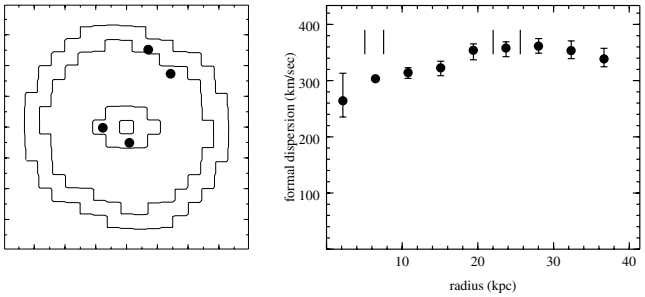

Figure 1. Left-hand panel: projected mass distribution of the CASTLES lens Q0957+561. The box size is 4×4 arcsec^2. The dots mark two doubly imaged systems. Right-hand panel: formal velocity dispersion $\sigma_{\rm lens}$. The vertical dashes mark the radial position of the lensed images. The same curve can be seen as second from top in Fig. 2.

Our sample consists of nine lensing galaxies from SLACS[1] data, nine from CASTLES[2] and two lensing clusters. We select these galaxy lenses using two criteria:

(1) the lensed images were either point-like sources or contain nearly point-like features, and
(2) the availability of $\sigma_{\rm obs}$ data.

Two cluster lenses with such properties are also included for comparison and contrast, since previous to this paper FP studies were carried out for small- and large-scale objects combined (e.g. Schaeffer et al. 1993). As an additional motivation, it is worth mentioning that Zwicky (1937) originally introduced gravitational lensing as a method to estimate masses of galaxy clusters.

The nine CASTLES lenses turn out to be a relatively inhomogeneous sample, a consequence of the fact that they spread over a large range in redshift and effective radii as well as lens radii.

The doubly imaged systems among the CASTLES lenses are **CFRS03.1077**, **HST15433** and **MG2016+112**. The effective radius of CFRS03.1077 is not known; hence, it is used for the analysis in Section 3 but not in Section 4. In HST15433, there is a neighbouring galaxy, but this is thought to only modestly perturb the estimated mass, according to JK07.

Q0957+561 is a special case, as there is a doubly imaged galaxy component in addition to the famous double quasar. The lensing galaxy is part of a cluster that contributes significantly to the large image separation (Garrett, Walsh & Carswell 1992). Consequently, a position below the general trend in a mass-to-light analysis is expected. This lens is an excellent example for the consequences of possibly yet unknown image systems. The considerations following in Section 3 for $\sigma_{\rm lens}$–$\sigma_{\rm obs}$ are carried out for two different image configurations: on the one hand, the two-double-image system shown in Fig. 1, and on the other hand a single-double system.

The quads from the CASTLES catalogue are **B0047−2808**, **PG1115+080**, **HST14176**, **B1608+656** and **Q2237+030**. B0047−2808 appears to have a double-component source, but this is probably not important for macro models. PG1115+080 has measured time delays and it is also part of a group, which contributes with a significant external shear. Neither of these were used for the models of this paper; if these are included, the lens models tend to become rounder, but $\sigma_{\rm lens}$ changes only by 5 to 10 per cent, which is insignificant for the present study. For the complex lens B1608+656, the measured time delays are used and make a more significant difference to the lens models. The lens Q2237+030 is actually the bulge of a barred galaxy. In the present study, the bulge is treated as an early-type galaxy. HST14176 is a part of a cluster, which is not included in the models. Another possible problem is a large uncertainty in the effective radius.

Several of these lenses have been studied individually in great detail. Different papers sometimes disagree on the slope of the profile (e.g. Treu & Koopmans 2002; Read, Saha & Macciò 2007, for PG1115+080), but agree on the enclosed mass. Hence, the effect on $\sigma_{\rm lens}$ would be small.

SLACS lenses populate a redshift range from 0.05 to 0.5. Due to smaller mean effective radii and lens redshifts, as a consequence of a limited aperture (3 arcsec) radius of SDSS fibres, the sample of nine SLACS lenses appears to be more clustered in mass-to-light plots than the CASTLES sample and has therefore a smaller rms. The SLACS lenses we use are a subset of the full SLACS sample for which point-like features are identified (Ferreras et al. 2008).

The doubly imaged systems among the SLACS lenses are **J0037−094**, **J0912+002**, **J1330−014** and **J2303+142**. All of them are quite typical with biases according to their observation method. J1330−014 is the nearest lens with $z = 0.08$ and shows the smallest $\sigma_{\rm obs}$. Among these lenses, J0912+002 takes a special position. It consists of two long arcs which are represented in this work as four doubles. Moreover, this lensing galaxy has the highest $\sigma_{\rm obs}$ among all lenses of our sample.

Quadruply imaged systems are found for the SLACS lenses **J1205+491**, **J1636+470** and **J2300+002**. Apart from J1636+470, all SLACS lenses have a larger kinematic velocity dispersion than lens velocity dispersion. The mean kinematic velocity dispersion $\langle\sigma_{\rm obs}\rangle$ of our SLACS sample is 10 per cent higher than $\langle\sigma_{\rm obs}\rangle$ of CASTLES lenses.

Also, **J0737+321** and **J0956+510** are thought to be quads, but in each of these only three images are used, as the astrometry of the faintest image was too uncertain. J0737+321 is with $z = 0.32$ the most distant in our SLACS subsample and belongs to higher z lenses in the whole catalogue.

Finally, we consider the two lensing clusters **ACO 1689** and **ACO 2667**.

ACO 1689 has a very large number of multiply imaged systems found by Broadhurst et al. (2005). In the present work, this cluster is modelled by a set of two five-image systems, six three-image systems and one double. The additional systems are known to affect only details (Saha, Williams & Ferreras 2007). Note that there are many more imaged sources, but adding those to the model does not change $M_{\rm lens}$, i.e. the mass model is tightly constrained by this set of image systems. The kinematic line-of-sight velocity dispersion $\sigma_{\rm obs} = 1400$ km s^{-1} of galaxies within the cluster was taken from Łokas et al. (2006) for a subset of 130 galaxies in the inner region of the cluster with velocities $|v| < 3000$ km s^{-1}, which most likely contains the biggest mass fraction responsible for the lensed images. This average value applies for a radius of around 400 kpc, a region where the formal velocity dispersion seems to be sufficiently flat and in which roughly half of the projected radii of the 130 galaxies considered in Łokas et al. (2006) are to be found. Furthermore, the value is not too far away from the Einstein radius or outermost image position of around 240 kpc. In order to estimate the I-band magnitude of the cluster, the 130 brightest out of 840 galaxies are taken from a cluster survey of Molinari, Buzzoni & Chincarini (1996) for which the Gunn g, r and i magnitudes were provided. Together with K-correction, evolution correction and galactic extinction we obtain $L_I = 2.82 \times 10^{12}\,{\rm L}_\odot$.

[1] http://www.slacs.org – the full set includes about 70 lenses, but image data were only made available for a small subset.
[2] http://cfa-www.harvard.edu/glensdata/.

ACO 2667: for this cluster, three three-image systems and one double were known to derive the formal mass-only related velocity dispersion curve. The kinematic velocity dispersion $\sigma_{\rm obs} = 960^{+190}_{-120}$ km s^{-1} of this lens was determined by Covone et al. (2006) from a sample of 21 galaxies in the inner region of the lensing cluster with a radius of $110\,h_{70}^{-1}$ kpc, which is in the same order of magnitude as $R_{\rm lens} = 98\,h_{72}^{-1}$ kpc. However, since photometric data for estimating the total flux of galaxies within the cluster were not available, ACO 2667 is not included in the mass-to-light plots of Section 4 and consequently there was no need to determine $R_{\rm eff}$ for the mass estimate.

The above lensing data are modelled using the PIXELENS program[3] (Saha & Williams 2004; Coles 2008). PIXELENS reconstructs the projected mass in a pixelated manner by solving a set of linear constraint lensing equations on the mass distribution by means of the given image positions, the redshifts of lens and source, the Hubble time (herein $h = 0.72$ is always assumed) and optionally the time delays between the lensed images. There are certain requirements for the mass distribution to be fulfilled. It has to be non-negative, centrally concentrated, with a local density gradient pointing less than 45° away from the centre, inversion symmetric (optional), it must not have a pixel which is twice the sum of its neighbours except possibly the central pixel and the circularly averaged mass profile needs to be steeper than $R^{-0.5}$, where R is the projected radius. Hence, an underdetermined set of equalities and inequalities is obtained. Subsequently, a Monte Carlo approach is used to sample over the mass map in order to determine an ensemble of lens models, for which the ensemble average appears to be the best single model representation. Of course all the uncertainties on any parameter can be derived from this model ensemble.

Since PIXELENS has been extensively tested in other papers, we will not get into details, but the following two points are worth noting.

(1) For tests of the recovery of simulated galaxy lenses, see Read et al. (2007).

(2) For the recovery of gross features of even extended lens structures from the information encoded in the image positions of lensed objects, see Saha & Williams (2001) and Ferreras et al. (2008).

For each lens, an ensemble of 100 mass maps with 21×21 pixels each has been computed, from which the mass profile and therewith the formal velocity dispersion $\sigma_{\rm lens}$ is derived with a 90 per cent uncertainty, as one can see for example for the lens Q0957+561 in Fig. 1. In Appendix B, we compare the average of an ensemble containing 100 models with larger ensembles containing up to 10 000 models to find that already small ensembles are sufficient to determine a fairly exact velocity dispersion. Since $\sigma_{\rm lens}(R)$ is not sensitive to ensemble enlargement, the number of models is fixed to 100 throughout this analysis.

Two points shall be emphasized here. First, the error bars in the right-hand panel of Fig. 1 represent the model dependence for an ensemble of 100 models and, as one can see, it is not large. Secondly, it is sometimes stated that the enclosed mass $M(<R)$ is known for $R = R_{\rm Ein}$, the Einstein radius and unknown for any other R, but this is oversimplified. In fact, $M(<R)$ has some model dependence at all R, but is minimal at $R_{\rm Ein}$. $\sigma_{\rm lens}(R \neq R_{\rm Ein})$ has a larger uncertainty than $\sigma_{\rm lens}(R_{\rm Ein})$, but is still fairly well constrained, as one can see in Fig. 1. The velocity dispersion at the radial position of the outermost image $\sigma_{\rm lens}(R_{\rm lens})$ as a quantity, which is as well constrained as $R_{\rm Ein}$, is basic to this paper.

The PIXELENS input files, mass maps as well as the formal velocity dispersion curves can be found in Appendix B of the online version of this paper. Note that for lensing clusters the velocity dispersion of the galaxies on their orbit around the centre of the cluster is considered instead of the stellar velocity dispersion as in the case of lensing galaxies. The references for all the lenses and further details can be seen in Table B1.

3 $\sigma_{\rm LENS}$ VERSUS $\sigma_{\rm OBS}$

The formal velocity dispersion curves $\sigma_{\rm lens}(R)$ illustrated in Fig. 1 for the lens Q0957+561 are now computed for all the lenses. Fig. 2 shows all these curves except for the cluster, which are excluded for the sake of readability and their comparatively high $\sigma_{\rm lens}$ values.

In the following, we concentrate on the formal velocity dispersion at a radius of the outermost image position $\sigma_{\rm lens}(R_{\rm lens})$ and at the effective radius $\sigma_{\rm lens}(R_{\rm eff})$. Concerning the latter, we cannot take for granted that the velocity dispersion curve at effective radii is still sufficiently flat. Because of this, when considering $\sigma_{\rm lens}(R_{\rm eff})$ we exclude the lenses Q2237, HST15433, J0737, J0912, CFRS03 and J0956, for which this condition is *not* fulfilled.

In terms of absolute values, the curves for CASTLES lenses extend in average to larger radii whereas the curves of SLACS lenses are smaller due to a limited aperture of the SDSS fibres. Note that seven SLACS lenses and three CASTLES lenses show a clear cuspy shape of the formal velocity dispersion curve towards inner radii as it is the case for the majority of early-type galaxies also in other velocity dispersion field studies (e.g. Coccato et al. 2009). However, in some cases anomalous galaxies exhibit a rising velocity dispersion profile, which might be related to the presence of a disc

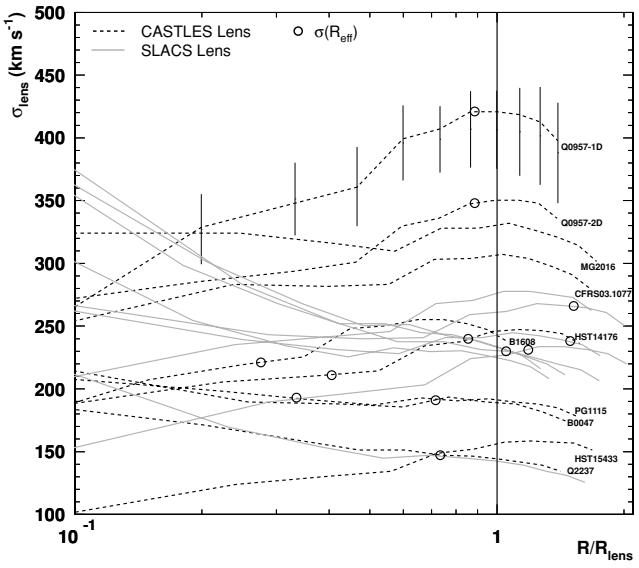

Figure 2. Formal velocity dispersion curves for all the galaxies. The grey solid lines denote SLACS lenses, the black dashed lines CASTLES lenses. For the sake of readability, the error bars, indicating the range of ensemble models, are shown only for one velocity dispersion curve. The radial scale is normalized to the radius of the respective outermost image $R_{\rm lens}$ which is indicated by the horizontal solid line. Open circles denote the effective radius provided it is located in a fairly flat region of the velocity dispersion curve. Q0957 is shown twice in this plot: Q0957-1D models one doubly imaged source, while Q0957-2D models two doubly imaged sources.

[3] Available from http://www.qgd.uzh.ch/projects/pixelens/.

according to Coccato et al. (2009). Additionally, the pixelated approach causes a variety of differently shaped velocity dispersion profiles differing especially in central regions. This leads consequently to large error bars and a decreased sensitivity in the centre, rendering an interpretation of the profiles at smaller radii rather difficult.

It should be emphasized that the comparison of either $\sigma_{\rm lens}(R_{\rm lens})$ or $\sigma_{\rm lens}(R_{\rm eff})$ with $\sigma_{\rm obs}$ measured within an aperture is a proper procedure, since $R_{\rm lens}$ is in average less than a factor of 2 different from the aperture radius, and for most lenses $\sigma_{\rm lens}$ remains unchanged. For J0737, J1205, J1330 and J2300, the formal velocity dispersion curve ends before reaching the radius of 3 arcsec, i.e. the mass does not contribute to the lensing effect, but nevertheless $\sigma_{\rm obs}$ can be taken as an indicator for the real velocity dispersion. With other words, the velocity dispersion measurements at aperture radius are probably not representative since the main mass of the lens is smaller.

Comparing the curves labelled Q0957-1D and Q0957-2D shows the probable effect of adding formerly undiscovered image systems. As for Q0957, $\sigma_{\rm lens}(R)$ varies considerably when a formerly unseen doubly imaged system is added. This also affects the relation between $\sigma_{\rm lens}(R_{\rm lens})$ or $\sigma_{\rm lens}(R_{\rm eff})$ and the kinematic velocity dispersion $\sigma_{\rm obs}$.

Both $\sigma_{\rm lens}(R_{\rm lens})$ and $\sigma_{\rm lens}(R_{\rm eff})$ plotted against $\sigma_{\rm obs}$ can be seen in Fig. 3. The comparison between the observed kinematic velocity dispersions and the mass-only related velocity dispersions reveals how virialized the lenses are, because $\sigma_{\rm lens} \approx \sigma_{\rm obs}$ is another representation of the virial theorem in equation (6). We constrain the fit by fixing it to the (0, 0) point, because a bias would have no physical relevance. For $\sigma_{\rm lens}$ values at effective radius instead of the radius of the outermost image position $R_{\rm lens}$, the scatter around the best fit decreases considerably. Although all $\sigma_{\rm lens}(R_{\rm eff})$ are within the error bars of $\sigma_{\rm lens}(R_{\rm lens})$, changing the radii for the determination of the $\sigma_{\rm lens}$–$\sigma_{\rm obs}$ relation might consequently be the right thing to do, since therewith the relation is build on a common basis.

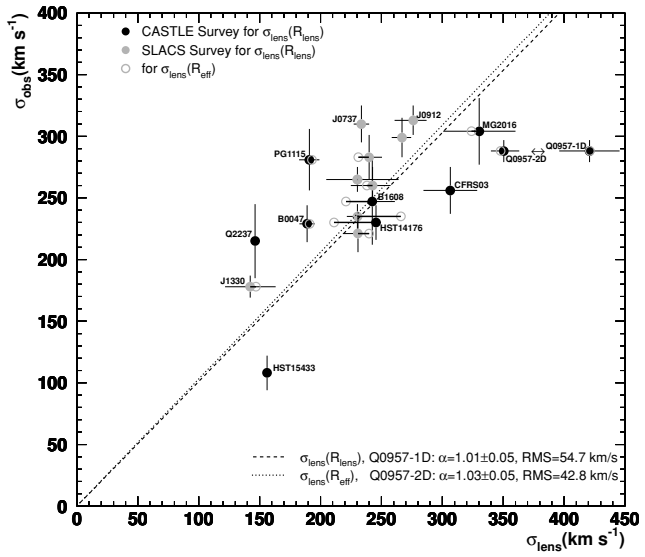

Figure 3. $\sigma_{\rm lens}$–$\sigma_{\rm obs}$ plot for all the galaxy lenses. The filled circles refer to formal velocity dispersions $\sigma_{\rm lens}$ measured at outermost image $R_{\rm lens}$. The open circles show $\sigma_{\rm lens}(R_{\rm eff})$. Note that as in Fig. 2 Q0957 is shown twice for different image systems. The dashed (dotted) line represents the fit for the solid (open) circles including Q0957-1D (Q0957-2D).

Furthermore, we included the two-double [two-dimensional (2D)] and the one-double [one-dimensional (1D)] system of lens Q0957 in Fig. 3 to demonstrate the grave difference in $\sigma_{\rm lens}$ of the former outlier, reducing the rms in the $\sigma_{\rm lens}$–$\sigma_{\rm obs}$ plot from 55 km s^{-1} for the $\sigma_{\rm lens}(R_{\rm lens})|_{\rm 1D}$ fit to 43 km s^{-1} for the $\sigma_{\rm lens}(R_{\rm eff})|_{\rm 2D}$ fit. We conclude that generally a more complete lens system is to be favoured, and henceforth we only consider Q0957-2D. The linear best fits fixed to the origin for $\sigma_{\rm lens}(R_{\rm eff})$ and $\sigma_{\rm lens}(R_{\rm lens})$ yield

$$\sigma_{\rm obs} = (1.03 \pm 0.05) \times \sigma_{\rm lens}(R_{\rm eff}), \tag{8}$$

$$\sigma_{\rm obs} = (1.04 \pm 0.04) \times \sigma_{\rm lens}(R_{\rm lens}). \tag{9}$$

As an aside, the y error bars plotted in Fig. 3 are the observational errors taken from Koopmans & Treu (2003), Treu & Koopmans (2004), Tonry & Franx (1999), Tonry (1998), Ohyama et al. (2002), Koopmans et al. (2003), Koopmans & Treu (2002) and Foltz et al. (1992) for the CASTLES lenses and Bolton et al. (2006) for SLACS lenses. The x error bars represent the statistical errors of the formal velocity dispersion for an ensemble of 100 models of possible mass distributions. Thus, the rather small error bars can be understood as a relatively model-independent lensing mass and formal velocity dispersion. The errors are taken from a radius closest to $R_{\rm lens}$, since the pixelated approach only allows for discrete steps in radius. One could argue about the significance of these errors, because changes in the image positions or lost information like additional image systems or mass contamination of the light path can lead to fairly different results.

However, the fits for $\sigma_{\rm obs}(\sigma_{\rm lens})$ (equations 8 and 9) make clear that a one-to-one correlation between $M_{\rm lens}$ and $M_{\rm vir}$ of the lensing galaxy is probable. It is important to know whether our sample is dominated by a certain kind of model far from $\rho(r) \sim r^{-2}$ corresponding to a constant $\sigma_{\rm lens}$. For that we can study the correlation between the ratios $\sigma_{\rm lens}/\sigma_{\rm obs}$ and $R_{\rm lens}/R_{\rm eff}$. In consideration of the virial theorem, one can state the following.

If there is an (anti)correlation between $\sigma_{\rm lens}/\sigma_{\rm obs}$ and $R_{\rm lens}/R_{\rm eff}$, the density profile $\rho(r)$ of the lens should be (flatter) steeper than r^{-2}.

Fig. 4 shows this relation for both $\sigma_{\rm lens}(R_{\rm lens})$ and $\sigma_{\rm lens}(R_{\rm eff})$. As for the first, the best fit shows a positive trend with large error bars. For $\sigma_{\rm lens}(R_{\rm eff})$, the positive trend is insignificant and the opposite result is *not* excluded by the error bars. By neglecting the outlier MG2016 with a possibly underestimated $R_{\rm eff}$, as will be discussed in Section 4, one finds the inverse trend to be likewise significant. Nevertheless, it needs to be emphasized that by excluding only one of the labelled outliers in Fig. 4 the slope is strongly affected and can change its algebraic sign. Thus, we cannot retrieve a strongly significant statement. In such exclusion scenarios, we obtain slopes consistent with constant σ ratio. Our sample of early-type lensing galaxies for $\sigma_{\rm lens}(R_{\rm lens})$ [$\sigma_{\rm lens}(R_{\rm eff})$] is clustering around a mean of 1.3 ± 0.3 (1.6 ± 0.3) in $R_{\rm lens}/R_{\rm eff}$ and around 0.91 ± 0.04 (0.96 ± 0.06) in $\sigma_{\rm lens}/\sigma_{\rm obs}$ excluding MG2016 because of its extraordinarily high $R_{\rm lens}/R_{\rm eff}$ ratio. Since we cannot find any type of correlation throughout our sample, we can summarize that $\sigma_{\rm lens}$ is model-independent.

Extending the $\sigma_{\rm obs}$–$\sigma_{\rm lens}$ plot in Fig. 3 to 100 kpc scale, as to be seen in Fig. 5, we can find that lensing clusters fit quite well to the previously found correlations for $\sigma_{\rm obs}(\sigma_{\rm lens})$ (equations 8 and 9).

Going from an assumed isothermal r^{-2} profile to a Hernquist profile makes the velocity dispersion of equation (6) change to $\sigma_{\rm h}$ shown in equation (A1) of Appendix A along the lines of Hernquist (1990). This step yields a change of less than 19 per cent of $\sigma_{\rm lens}$ for most lenses, apart from few exceptions like P1115, which turned out

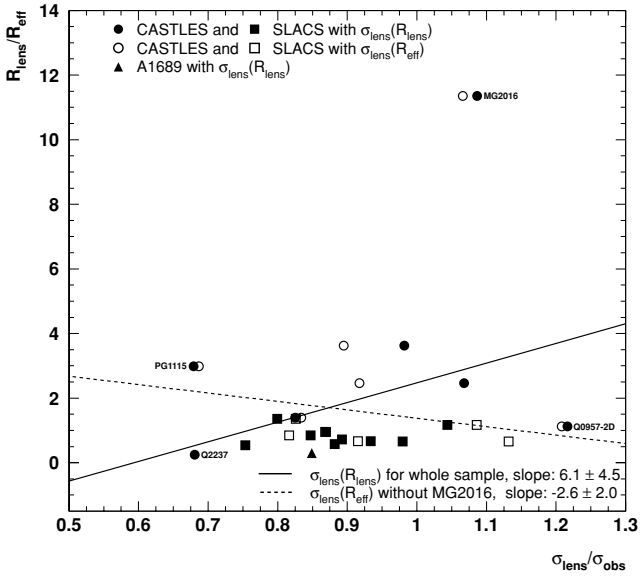

Figure 4. Plot of $R_{\rm lens}/R_{\rm eff}$ against $\sigma_{\rm lens}/\sigma_{\rm obs}$. The lines indicate extreme scenarios of formal fits for our sample of early-type galaxies which show large errors. For the $\sigma_{\rm lens}(R_{\rm eff})$ fit of the whole sample, the positive trend is insignificant. The trend inverts when excluding MG2016. In other words, there is neither correlation nor anticorrelation, meaning that in average the density profile for all lenses is consistent with an isothermal ellipsoid.

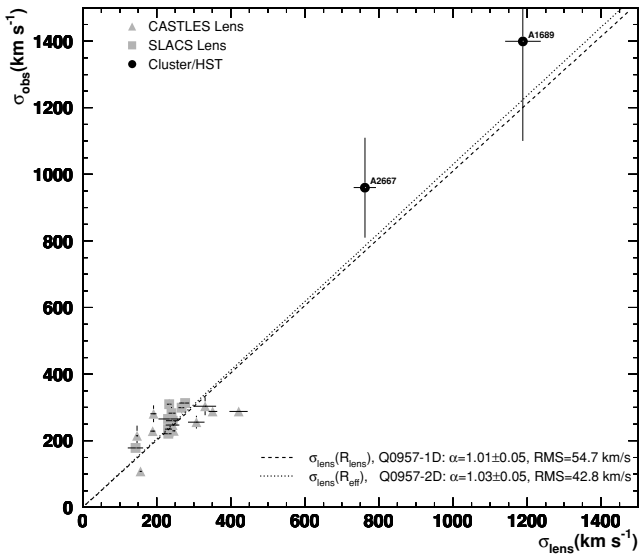

Figure 5. Like Fig. 3, but with the two clusters ACO 1689 and ACO 2667 included. The straight line fits do not include the clusters. The relation between $\sigma_{\rm obs}$ and $\sigma_{\rm lens}$ extends to cluster scales.

to be an outlier already in Fig. 4. Furthermore, cluster ACO 2667 shows a velocity dispersion increased by 33 per cent. In general, central regions of galaxy clusters are best fitted by a Hernquist profile (Hernquist 1990) for the stellar component of the inner cD galaxy and an NFW model (Navarro, Frenk & White 1996) for the dark matter component, shown by for example Padmanabhan et al. (2004). That is why we can expect significant changes going from $\sigma_{\rm lens}$ to $\sigma_{\rm h}$ on larger scales. However, fitting the $\sigma_{\rm lens}$–$\sigma_{\rm obs}$ relation for a Hernquist profile as done before with an isothermal model for $\sigma_{\rm lens}$ reveals a slightly steepened slope compared to equation (9) of (1.13 ± 0.04). The clusters still agree to this relation within the error bars.

The dynamical state of galaxy clusters is hard to determine. There are many contradictory investigations on this topic. Optical and X-ray data on the one hand indicate ongoing formation processes on substructure level (e.g. Stein 1997; Solanes, Salvador-Solé & González-Casado 1999), which should be considered in the estimates of $M_{\rm vir}$. On the other hand, statistical comparisons of different mass estimates from optical and X-ray observations and weak lensing show perfect agreement on scales much greater than the core radius $R_{\rm core}$ (e.g. Wu & Fang 1997). Still, on scales of core radii there are discrepancies between X-ray and mass measurements by means of weak lensing. Allen (1998) suggests to consider substructure and line-of-sight alignments of material towards the cluster cores since they will increase the lensing masses without affecting X-ray data and to take account of the dynamical activity which might cause the X-ray analyses to overestimate $R_{\rm core}$. Xu, Fang & Wu (2000) take this apparent dichotomy as an indicator of the transition from pre-virialization to virialization. In this paper, however, we can probe the virialization state for the two clusters at $R_{\rm lens}$, which is in both cases not far away from $R_{\rm core}$. The core radii of the X-ray-selected ACO 2667 and ACO 1689 are about (76 ± 8) kpc (Covone et al. 2006) and (80 ± 15) kpc (Allen 1998), respectively. Thus, with $\sigma_{\rm lens}$ at $R_{\rm eff} = 98$ kpc for ACO 2667 we already probe the core region. For ACO 1689, $R_{\rm eff}$ is roughly 238 kpc, which is three times the given core radius. By adjusting to smaller scales, $\sigma_{\rm lens}(R_{\rm core})$ becomes $\sim$1000 km s^{-1} and marginally fails the relations (8) and (9). It should be emphasized that unlike the sample of lensing galaxies ACO 1689 $R_{\rm core}$ is *not* in a sufficiently flat region of $\sigma_{\rm lens}$ and thus not comparable with the relations for which this was a requirement. Since strong lensing unveils mass regardless of underlying dynamics, one can summarize that also in view of findings from previous studies clusters in a wide range of radii can be regarded as virialized.

Nevertheless, the correlation between the kinematic velocity dispersion $\sigma_{\rm obs}$ and $\sigma_{\rm lens}$ is hard to decipher. First, the scatter around a best fit that is smaller (larger) than the scatter around the FP in the ($R_{\rm eff}$, σ, I) parameter space can be understood as a hint on a basically mass-dependent (stellar-dynamics-dependent) $\sigma_{\rm obs}$. Of course it can also be seen as a merely statistical scatter that is influenced by a possibly biased lens sample. This allows for drawing the following conclusions.

(1) The small scatter and the slope of the best fit of $\sim$1 make $\sigma_{\rm lens}$ a good surrogate for $\sigma_{\rm obs}$, which is independent of a particular density profile model.
(2) The included elliptical galaxies are thus virialized.
(3) The relation can be extended to larger scale objects like clusters, as we can see in Fig. 5.

With this in hand, we now want to analyse the mass-to-light relationship for the given sample and compare it to the governing FP of early-type galaxies.

4 MASS-TO-LIGHT RATIO AND THE FUNDAMENTAL PLANE

As a first step to a mass-to-light relation for this sample of early-type lensing galaxies, we *K*-correct given *I*-band magnitudes (centred on 814 nm) and SDSS-*I*-band magnitudes (centred on 753 nm) in *AB* units to rest-frame *I*-band since they provide the most complete set of magnitudes for our sample. These are taken from the CASTLE

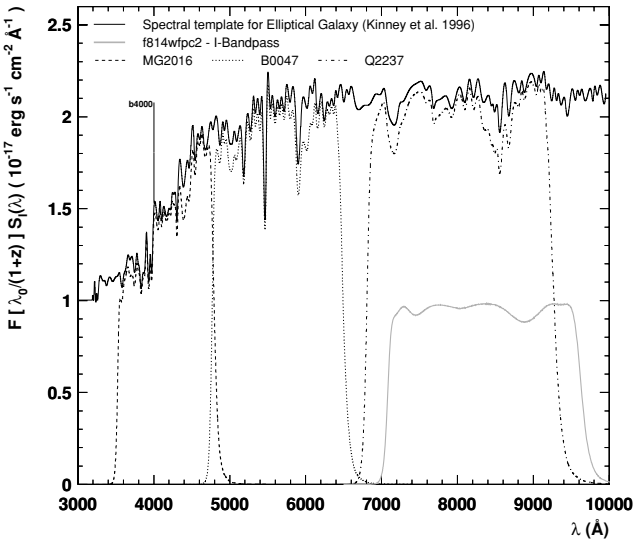

Figure 6. Visualization of *K*-correction: the black solid curve shows the flux template of an elliptical galaxy. The grey solid line represents the *HST* WFPC2 *I* bandpass taken from http://www-int.stsci.edu/instruments/wfpc2/Wfpc2_thru/. The dashed curves are showing the denominator of the integrand in equation (10) for three lenses: MG2016 ($z = 1.01$; dashed line), B0047 ($z = 0.485$; dotted line) and Q2237 ($z = 0.04$; dash–dotted line).

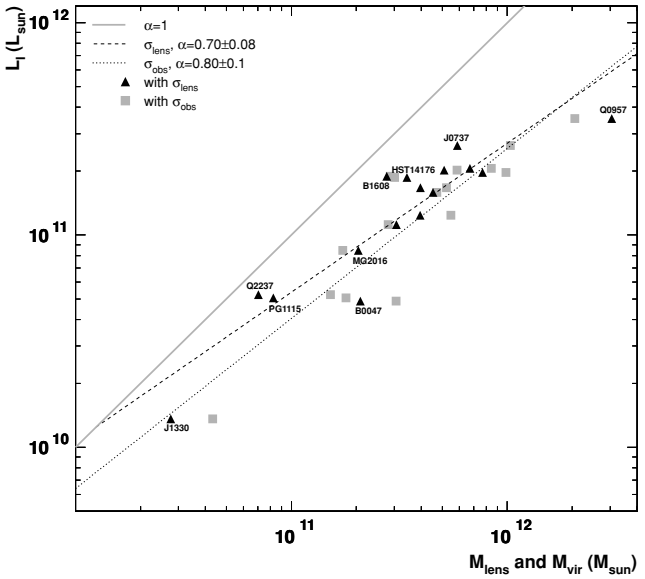

Figure 7. Lensing mass and virial mass against *I*-band luminosity for all galaxies. The triangles denote masses calculated using $\sigma_{\rm lens}$. The squares refer to masses calculated with $\sigma_{\rm obs}$. The best fits for $M^{\alpha} \propto L$ are plotted for $\sigma_{\rm lens}(R_{\rm lens})$ (dashed line) and for $\sigma_{\rm obs}$ (dotted line). The solid line refers to a constant *M*/*L* ratio.

Survey homepage[4] and Bolton et al. (2006). In the case of the galaxy cluster ACO 1689, we obtain the overall magnitude by summing over the fluxes of the galaxy content using the catalogue of Molinari et al. (1996). Hence, the *K*-correction is based on SDSS, *Hubble Space Telescope* (*HST*) and European Southern Observatory (ESO) spectral templates.[5]

We carry out the *K*-correction from first principles in preference to a black box program. Following Oke & Sandage (1968), we compute the *K*-corrected flux according to

$$K_x = 2.5\log(1+z) + 2.5\log\left\{\frac{\int_0^\infty F(\lambda_0)S_x(\lambda)\mathrm{d}\lambda}{\int_0^\infty F[\lambda_0/(1+z)]S_x(\lambda)\mathrm{d}\lambda}\right\}, \quad (10)$$

where K_x denotes the *K*-correction for the x band expressed in magnitudes. The bandwidth is smaller in the redshifted galaxy, which leads to the first term in (10). A source spectrum $F(\lambda)$ is redshifted through fixed spectral-response bands S_x or bandpasses, respectively, of the detector. The flux at an effective wavelength in the rest frame of a galaxy of redshift z, transformed from the effective wavelength λ_0 of the detector by $\lambda_0/(1+z)$, will differ from the flux of a galaxy at rest. This leads to the second term in (10). Fig. 6 visualizes the denominator of the integrand in equation (10), where the *I* bandpass is multiplied by the redshifted flux template of an elliptical galaxy taken from Kinney et al. (1996). As an aside, the apparent SDSS magnitudes are on an *AB* basis within 3 per cent, which only leads to minor corrections and is therefore neglected in the following analysis. Note that the *K*-correction is realized with the exact template for $\lambda < 570$ nm. For higher wavelengths, we assumed a constant flux for the sake of simplicity. The deviations resulting from this approximation are even in the worst case of a hardly redshifted galaxy in the upper λ range like Q2237 of only 0.3 per cent for L_I. This leads to negligible corrections for all following quantities. Furthermore, galactic extinction corrections according to Schlegel, Finkbeiner & Davis (1998) are applied to the fluxes. The luminosities are calculated in units of solar luminosities according to an *AB* magnitude[6] $\mathrm{I}_\odot = 4.57$ for WFPC2 data and $\mathrm{i}_\odot = 4.48$ for SDSS data calculated along the lines of Fukugita, Shimasaku & Ichikawa (1995). Subsequently, we correct for passive *M*/*L* evolution with a slope of

$$\frac{\mathrm{d}\log M/L_I}{\mathrm{d}z} = -0.397$$

inferred by stellar population synthesis models taken from Bruzual & Charlot (2003).

Having the *I*-band luminosities L_I of all lenses in units of solar luminosities $\mathrm{L}_\odot$ and the velocity dispersions from Section 3, we can analyse the underlying mass-to-light relation. Fig. 7 shows the lensing mass $M_{\rm lens} = R_{\rm eff}\sigma^2_{\rm lens}(R_{\rm lens})$ and the virial mass $M_{\rm vir} = R_{\rm eff}\sigma^2_{\rm obs}$ plotted against *I*-band luminosity. The plot also provides a curve representing a constant *M*/*L* or according to equation (4) a ($\alpha = 1$) line, respectively.

A closer look at the *V*-band luminosities for selected galaxies reveals that HST14176, B1608 and MG2016 emerge as outliers with mass-to-light ratios $\lesssim$1. This can be explained by nearby groups and clusters (e.g. in the case of HST14176) or mass contamination influencing the path of light. Another reason can be uncertainties in the effective radii, as already mentioned in Section 3. If we take for HST14176 (MG2016) $R_{\rm eff} = 1.06$ (0.31) arcsec (Treu & Koopmans 2004) instead of the used 0.71 (0.22) arcsec (Rusin et al. 2003b), then $M_{\rm lens} = R_{\rm eff}\sigma^2_{\rm lens}$ would increase by a factor of $\sim$1.5 (1.4), since no grave changes in σ for a flat formal velocity dispersion

[4] http://cfa-www.harvard.edu/glensdata/.

[5] The spectral templates for Wide Field Planetary Camera 2 (WFPC2), SDSS ACS and ESO telescopes are taken from the STScI homepage http://www-int.stsci.edu/instruments/wfpc2/Wfpc2_thru/, http://stsci.edu/hst/acs/analysis/reference_files/synphot_tables.html and http://filters.ls.eso.org/efs/efs_fi.htm.

[6] Listed on http://www.ucolick.org/~cnaw/sun.html

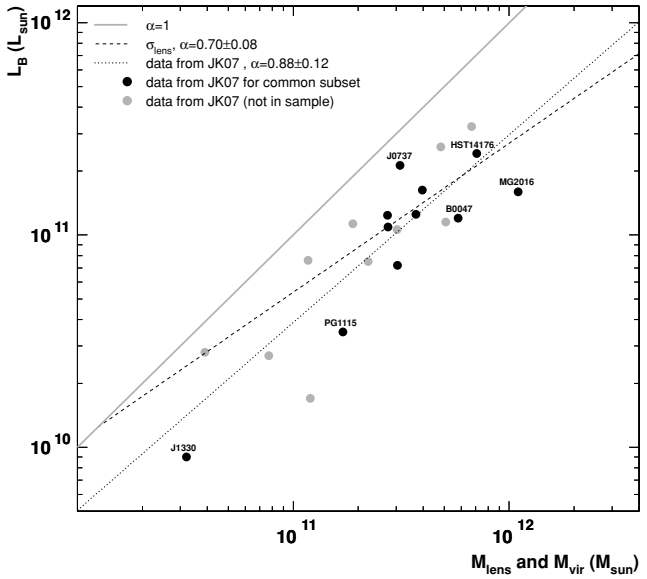

Figure 8. Mass-versus-light plot for data from JK07. The black circles denote a subset of lenses included in the lens sample of this paper. The grey circles are residual lenses. The dotted line represents the best fit for the whole data set taken from JK07. The dashed line refers to the $\sigma_{\rm lens}$ fit as seen in Fig. 7.

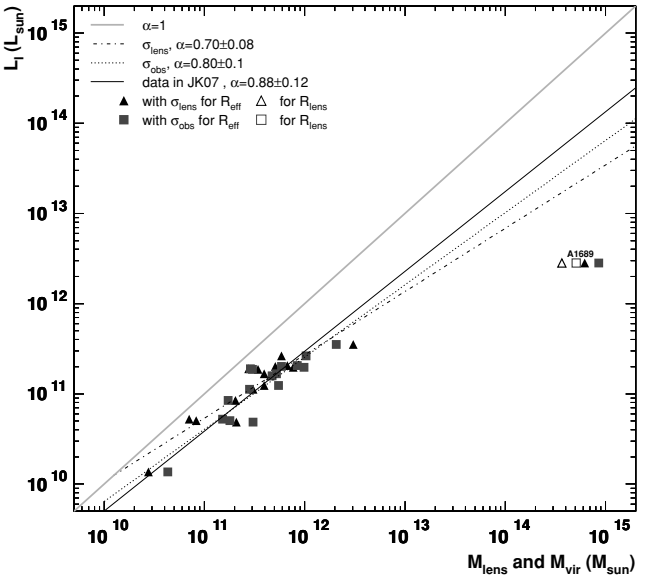

Figure 9. Like Fig. 7, but extended by cluster ACO 1689. As expected, clusters are not on the FP, because they have a higher mass-to-light ratio. Solid symbols denote masses calculated with $\sigma(R_{\rm eff})$ and open symbols denote masses calculated with $\sigma(R_{\rm lens})$.

curve are expected. This leads for HST14176 to a lensing mass of $5.14 \times 10^{11}\,{\rm M}_{\odot}$ instead of the former $3.43 \times 10^{11}\,{\rm M}_{\odot}$ which is then also in the V band clearly below the $(\alpha = 1)$ line. If such uncertainties are the true cause for comparatively high luminosities, then we also need to adjust $M_{\rm lens}$ and $M_{\rm vir}$ in Fig. 7. However, changing $R_{\rm eff}$ or excluding the problematic lenses from the fit has a negligible impact on the slope α using $M_{\rm lens}$ and only small impact using $M_{\rm vir}$, changing α from (0.80 ± 0.10) to (0.84 ± 0.10). It should be emphasized that we hold on to the data set of Rusin et al. (2003b), because it provides the effective radii computed on a common basis for the whole CASTLES subset of our lensing objects.

Both sets of data points for $\sigma_{\rm obs}$ and for $\sigma_{\rm lens}(R_{\rm lens})$ are fitted for the whole sample and reveal the slopes

$\alpha = (0.70 \pm 0.08)$ for $M_{\rm lens}$,

$\alpha = (0.80 \pm 0.14)$ for $M_{\rm vir}$.

It shows that $\alpha = 1$ is in any case clearly excluded. Fig. 7 shows the best fit for both $M_{\rm lens}$ and $M_{\rm vir}$. Note that the fits in the plot cannot be extrapolated to lower masses, which would mean that judging by the intersection with the $(\alpha = 1)$ line the luminous mass would overtake the total mass content. The plot and therewith also the FP of nearby lenses show that more massive galaxies have a larger dark matter fraction.

In Fig. 8, the lens sample from JK07 together with a best fit is shown. Their data from stellar-dynamical measurements on 22 early-type models contain a common subset with the present study. Note that the data in JK07 were given in B-band luminosities, which explain the shift of the data points towards lower luminosities in most cases. The fit for the whole JK07 sample yields a slope of $\alpha = 0.88 \pm 0.12$. As in Fig. 7, a curve indicating a constant mass-to-light relation is included.

From these plots, we can summarize that

(1) the slope of the best fit for $\sigma_{\rm obs}$ is consistent with the one for the lensing sample of JK07 within error bars,

(2) the slope of the fit for $\sigma_{\rm lens}$ is not consistent with the fit for data from JK07, although the error bars do overlap,

(3) only the fit for the JK07 sample is consistent with $\alpha = 1$,

(4) the slopes of the $\sigma_{\rm lens}$ and $\sigma_{\rm obs}$ fits (for the whole data set and for a reduced or, due to uncertainties in $R_{\rm eff}$, changed data set) are clearly excluding $\alpha = 1$ within their error bars and thus do not agree with a constant M/L ratio.

In Fig. 9, we extend determined mass-to-light relations to larger scales. For cluster-sized objects like ACO 1689, $R_{\rm eff}$ is of course not defined. Nevertheless, one can still use the mass quantity $R\sigma^2$ to compare the mass-to-light behaviour of early-type galaxies and clusters. The kinematic line-of-sight velocity dispersion $\sigma_{\rm obs} = 1400\ {\rm km\,s^{-1}}$ of galaxies within the cluster was taken from Łokas et al. (2006) for a subset of 130 galaxies in the inner region of the cluster with velocities $|v| < 3000\ {\rm km\,s^{-1}}$, which contains most likely the biggest mass fraction responsible for the lensed images. This average value applies for a radius of around 400 kpc, a region where the formal velocity dispersion seems to be sufficiently flat and in which roughly half of the projected radii of the 130 galaxies considered in Łokas et al. (2006) are to be found. Furthermore, the value is not too far away from the outermost image position of around 240 kpc. Therewith, $R_{\rm eff}\sigma^2_{\rm obs}(R_{\rm eff})$ and $R_{\rm eff}\sigma^2_{\rm obs}(R_{\rm lens})$ are determined.

The data points for the cluster deduced from the formal velocity dispersion $\sigma_{\rm lens}$ at $R_{\rm lens}$ and $R_{\rm eff}$ are included in Fig. 9. As expected, neither the relation $M^{\alpha} \propto L$ with $\alpha \approx 0.70$ nor with any other slope presented above does extend to clusters. As shown by Schaeffer et al. (1993), galaxy clusters follow indeed a different FP relation. We can make up a region in the mass-to-light plot for cluster-sized objects, which lies far below all previous lines and matches the findings of Schaeffer et al. (1993) for an FP consisting of 16 clusters. One should keep in mind that for early-type galaxies M/L can be a suitable dark matter versus baryon estimator because L tracks pretty much all baryons. But this is not a good approximation for clusters, whose total baryonic mass is generally believed to be made of 80 per cent hot diffuse gas and only 20 per cent galaxies (Fukugita,

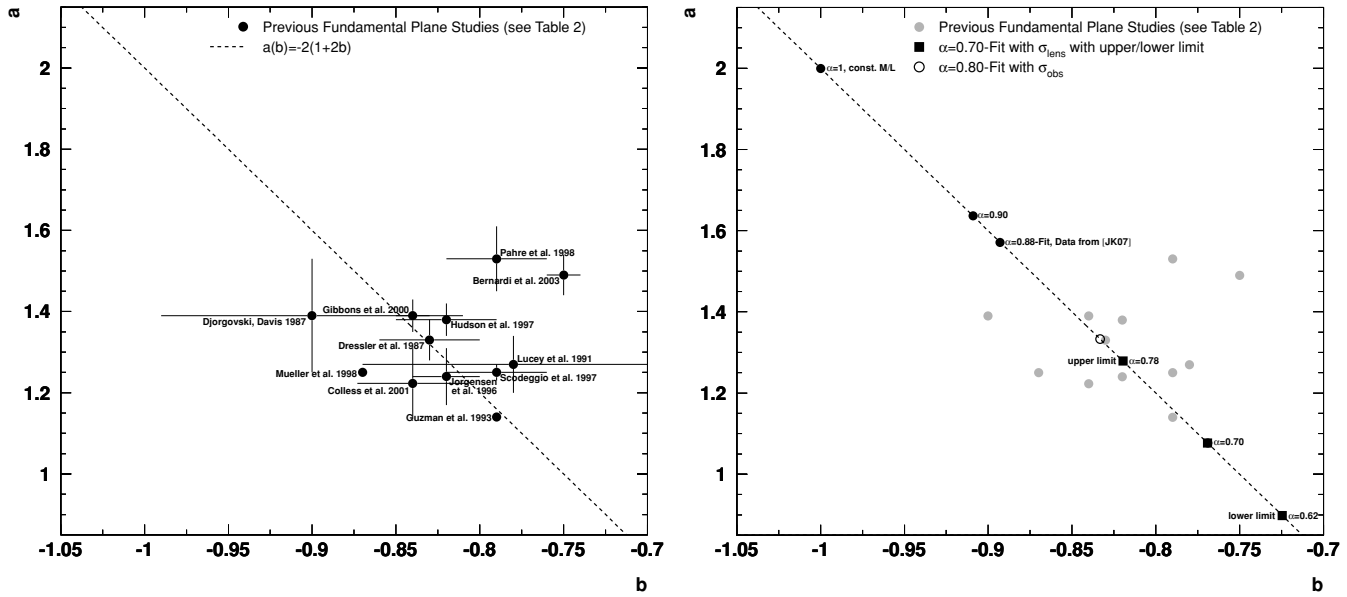

Figure 10. Left-hand panel: the a-b-parameter space according to equation (3). The dashed line represents the mass-to-light power index α for related a and b according to equation (5). The plot shows FP parameter from previous studies referenced in Table B2. The error bars are included as far as provided in the references. Right-hand panel: like left-hand plot, but with results from this paper. The squares mark upper, lower and mean values of the fit using $\sigma_{\rm lens}$ for the whole sample of early-type galaxies. The open circle denotes the fit using $\sigma_{\rm obs}$. The black filled circles denote other α values, like the Vanilla Plane or the fit for data from JK07. For the sake of readability and comparison, the grey filled circles corresponding to the data shown in the left-hand panel are included.

Hogan & Peebles 1998). In order to correct for this discrepancy, one might add the missing 80 per cent expressed in terms of luminosity. Hence, the luminosity of ACO 1689 is shifted to $1.4 \times 10^{13}\,{\rm L}_{\odot}$. Despite this correction, we obtain a value significantly below the given fits. Thus, clusters can nonetheless be regarded as highly dark matter dominated.

We can summarize that our results are in good agreement with most of the recent FP-type studies, as one can see in Fig. 10. In the two plots, the FP parameter study results of the references listed in Table B2 are presented (left-hand panel) together with the results of this paper (right-hand panel). Recovering the FP of early-type galaxies by means of the photometric-independent $\sigma_{\rm lens}$ shows that non-homologies like structural and orbital anisotropies, which might change the photometrically determined central velocity dispersion, have small to negligible impact on the FP tilt, as also shown by Cappellari et al. (2006).

The FP parameters of our analysis are determined in consideration of the relations $a = 2\alpha(2-\alpha)^{-1}$ and $b = -(2-\alpha)^{-1}$:

$$a = 1.08, \quad b = -0.77 \quad \text{for } \sigma_{\rm lens},$$

$$a = 1.33, \quad b = -0.83 \quad \text{for } \sigma_{\rm obs},$$

corresponding to $\alpha = 0.70 \pm 0.08$ and 0.80 ± 0.10, respectively. Upper and lower limits of the $\sigma_{\rm lens}$ fit are also drawn into the plot and plainly exclude the $M \propto L$ case of the Vanilla Plane.

Moreover, the FP parameters found in this study are conspicuously surrounded by the ones found in other studies (see Table B2). For example, in recent SDSS results for nearly 9000 early-type galaxies in a redshift range of $0.01 < z < 0.3$ the parameters are determined to $a = 1.49 \pm 0.05$ and $b = -0.75 \pm 0.01$ (Bernardi et al. 2003), and as an aside have no common α, since equation (5) does not hold. On the other hand, Dressler et al. (1987) in one of the first FP parameter studies present parameters, which are almost perfectly in agreement with the fixed a to b relation and a common α of $\sim$0.80, although measured separately. This value is verified in this paper by the mass-to-light relation found for $M_{\rm vir}$. It can be seen that (a, b) for the slope of the $\sigma_{\rm lens}$ fit is close to the results of Guzman, Lucey & Bower (1993), Colless et al. (2001), Jørgensen et al. (1996), Scodeggio, Giovanelli & Haynes (1997), Lucey, Bower & Ellis (1991) and Dressler et al. (1987) in the ascending order of distance in (a, b) space. Except for Hudson et al. (1997), Pahre, Djorgovski & de Carvalho (1998), Gibbons et al. (2000) and Bernardi et al. (2003), the errors of previous (a, b) studies, as far as they were given, overlap with the error bars in this study. In particular, the results of Jørgensen et al. (1996) and Colless et al. (2001) agree with the upper limit of α values from the $\sigma_{\rm lens}$ fit. However, the α estimate from the data set of JK07, which matches the result from Rusin et al. (2003b), can be excluded. Since for all previous FP-type studies kinematic velocity dispersion measurements are used, our findings suggest that the real underlying (a, b) values are even closer to the lower-right corner of Fig. 10.

5 CONCLUSION

We can summarize the findings of this paper as follows.

(1) Independent of the details of lens models, the lensing masses and virial masses basically agree, since $\sigma_{\rm lens} \approx \sigma_{\rm obs}$, as demonstrated in Section 3. This verifies the virial theorem.

(2) The relation between the lensing-inferred velocity dispersion $\sigma_{\rm lens}$ and the observed kinematic velocity dispersion $\sigma_{\rm obs}$ extends to cluster-sized lensing objects within rather large uncertainties originating from a poorly defined scale radius $R_{\rm eff}$ as shown up for the two galaxy clusters ACO 1689 and ACO 2667.

(3) Using the results for $\sigma_{\rm lens}(\sigma_{\rm obs})$ in Section 4, the lensing mass (virial mass) is calculated according to $M \approx R_{\rm eff}\sigma^2$. We find the mass-to-light relation $M_{\rm lens}^{0.70\pm0.08} \propto L$ for the whole sample and $M_{\rm vir}^{0.80\pm0.10} \propto L$ to be consistent with most other FP-type studies. We point out that the FP defined by using $\sigma_{\rm lens}(R_{\rm lens})$ is based on lensing velocity dispersions within $R_{\rm lens}$, which is not correlated to the

effective radius. In order to render the used quantities unequivocal, we analyse the change in $\sigma_{\rm lens}$–$\sigma_{\rm obs}$ switching from $R_{\rm lens}$ to $R_{\rm eff}$ and find only a marginally different slope, though a reduced scatter in the $\sigma_{\rm lens}$–$\sigma_{\rm obs}$ plot can be seen. A few lenses are problematic outliers due to observational uncertainties but excluding these does not effectively change the result. With $R \propto \sigma_{\rm lens}^{1.08}\, I^{-0.77}$, the FP of early-type galaxies is recovered, clearly excluding the Vanilla Plane. Thus, non-homology as a reason for the FP tilt can also be excluded.

(4) As shown for ACO 1689, clusters are far from the FP since they have a much higher dark matter fraction than early-type galaxies.

The FP tilt discovered by Dressler et al. (1987) and recovered in this study using $\sigma_{\rm lens}$ as a surrogate is an often discussed matter (see Table B2) in astrophysics. The reasons for the deviation from the Vanilla Plane are hard to resolve, because neither the mass-structure, the mass-to-light ratio nor the dark matter fraction is directly and independently observable. Until a consensus on the explanation for the FP is found, it is necessary to focus on quantities which are unequivocally related to a certain physical entity. For this purpose, $\sigma_{\rm lens}$ is proposed in this paper, since it fulfils the necessary condition of preserving the viriality for both elliptical galaxies and clusters.

ACKNOWLEDGMENTS

I would like to thank Prasenjit Saha for patiently answering my many lensing questions and giving useful suggestions on making this paper clearer. Many thanks to Ignacio Ferreras and Andrea Macció for all helpful suggestions, to Jonathan Coles for giving further insights in PIXELENS and Justin Read for useful discussions. Furthermore, I thank the Swiss National Science Foundation for financial support.

REFERENCES

Allen S. W., 1998, MNRAS, 296, 392
Bernardi M. et al., 2003, AJ, 125, 1866
Bolton A. S., Burles S., Koopmans L. V. E., Treu T., Moustakas L. A., 2006, ApJ, 638, 703
Bolton A. S., Burles S., Treu T., Koopmans L. V. E., Moustakas L. A., 2007, ApJ, 665, L105
Bolton A. S., Treu T., Koopmans L. V. E., Gavazzi R., Moustakas L. A., 2008, ApJ, 684, 248
Broadhurst T. et al., 2005, ApJ, 621, 53
Bruzual G., Charlot S., 2003, MNRAS, 344, 1000
Cappellari M. et al., 2006, MNRAS, 366, 1126
Coccato L. et al., 2009, MNRAS, 217
Coles J., 2008, ApJ, 679, 17
Colless M., Saglia R. P., Burstein D., Davies R. L., McMahan R. K., Wegner G., 2001, MNRAS, 321, 277
Covone G., Kneib J.-P., Soucail G., Richard J., Jullo E., Ebeling H., 2006, A&A, 456, 409
Djorgovski S., Davis M., 1987, ApJ, 313, 59
Dressler A., Lynden-Bell D., Burstein D., Davies R. L., Faber S. M., Terlevich R., Wegner G., 1987, ApJ, 313, 42
Ferreras I., Saha P., Williams L. L. R., 2005, ApJ, 623, L5
Ferreras I., Saha P., Burles S., 2008, MNRAS, 383, 857
Foltz C. B., Hewett P. C., Webster R. L., Lewis G. F., 1992, ApJ, 386, L43
Fukugita M., Shimasaku K., Ichikawa T., 1995, PASP, 107, 945
Fukugita M., Hogan C. J., Peebles P. J. E., 1998, ApJ, 503, 518
Garrett M. A., Walsh D., Carswell R. F., 1992, MNRAS, 254, 27P
Gibbons R. A., Fruchter A. S., Bothun G. D., 2000, in Courteau S., Strauss M. A., Willick J. A., eds, ASP Conf. Ser. Vol. 201, Cosmic Flows Workshop. Astron. Soc. Pac., San Francisco, p. 92
Graham A., Colless M., 1997, MNRAS, 287, 221
Guzman R., Lucey J. R., Bower R. G., 1993, MNRAS, 265, 731
Hernquist L., 1990, ApJ, 356, 359
Hudson M. J., Lucey J. R., Smith R. J., Steel J., 1997, MNRAS, 291, 488
Jiang G., Kochanek C. S., 2007, ApJ, 671, 1568 (JK07)
Jørgensen I., Franx M., Kjaergaard P., 1996, MNRAS, 280, 167
Keeton C. R., Kochanek C. S., Falco E. E., 1998, ApJ, 509, 561
Kinney A. L., Calzetti D., Bohin R. C., McQuade K., Storchi-Bergmann T., Schmitt H. R., 1996, ApJ, 467, 38
Koopmans L. V. E., Treu T., 2002, ApJ, 568, L5
Koopmans L. V. E., Treu T., 2003, ApJ, 583, 606
Koopmans L. V. E., Treu T., Fassnacht C. D., Blandford R. D., Supri G., 2003, ApJ, 599, 70
Łokas E. L., Prada F., Wojtak R., Moles M., Gottlöber S., 2006, MNRAS, 366, L26
Lucey J. R., Bower R. G., Ellis R. S., 1991, MNRAS, 249, 755
Molinari E., Buzzoni A., Chincarini G., 1996, A&AS, 119, 391
Müller K. R., Freudling W., Watkins R., Wegner G., 1998, ApJ, 507, L105
Navarro J. F., Frenk C. S., White S. D. M., 1996, ApJ, 462, 563
Ohyama Y. et al., 2002, AJ, 123, 2903
Oke J. B., Sandage A., 1968, ApJ, 154, 21
Padmanabhan N. et al., 2004, New Astron., 9, 329
Pahre M. A., Djorgovski S. G., de Carvalho R. R., 1998, AJ, 116, 1591
Read J. I., Saha P., Macciò A. V., 2007, ApJ, 667, 645
Rusin D., Kochanek C. S., Keeton C. R., 2003a, ApJ, 595, 29
Rusin D. et al., 2003b, ApJ, 587, 143
Saha P., Williams L. L. R., 2001, AJ, 122, 585
Saha P., Williams L. L. R., 2004, AJ, 127, 2604
Saha P., Williams L. L. R., Ferreras I., 2007, ApJ, 663, 29
Schaeffer R., Maurogordato S., Cappi A., Bernardeau F., 1993, MNRAS, 263, L21
Schlegel D. J., Finkbeiner D. P., Davis M., 1998, ApJ, 500, 525
Scodeggio M., Giovanelli R., Haynes M. P., 1997, AJ, 113, 2087
Solanes J. M., Salvador-Solé E., González-Casado G., 1999, A&A, 343, 733
Stein P., 1997, A&A, 317, 670
Tonry J. L., 1998, AJ, 115, 1
Tonry J. L., Franx M., 1999, ApJ, 515, 512
Treu T., Koopmans L. V. E., 2002, MNRAS, 337, L6
Treu T., Koopmans L. V. E., 2004, ApJ, 611, 739
Treu T., Koopmans L. V., Bolton A. S., Burles S., Moustakas L. A., 2006, ApJ, 640, 662
Trujillo I., Burkert A., Bell E. F., 2004, ApJ, 600, L39
Wu X.-P., Fang L.-Z., 1997, ApJ, 483, 62
Xu W., Fang L.-Z., Wu X.-P., 2000, ApJ, 532, 728
Zwicky F., 1937, ApJ, 86, 217

APPENDIX A:

For a Hernquist profile, the velocity dispersion $\sigma_{\rm h}$ of a projected distribution is

$$\sigma_{\rm h}^2(R_{\rm lens}) \sim \frac{GM_{\rm vir}^2}{aM_{\rm lens}} \frac{(1-s^2)^2}{[(2+s^2)X(s)-3]} \left\{ \frac{1}{2} \frac{1}{(1-s^2)^3} \times [-3s^2X(s)(8s^6-28s^4+35s^2-20) - 24s^6+68s^4+65s^2+6] - 6\pi s \right\} \quad \text{(A1)}$$

with $s = R/a$, whereas a denotes a scalelength and

$$X(s) = \begin{cases} \frac{\operatorname{sech}^{-1} s}{\sqrt{s^2-1}} & \text{for} \quad 0 \le s \le 1 \\ \frac{\cos^{-1} s^{-1}}{\sqrt{s^2-1}} & \text{for} \quad 1 \le s \le \infty \end{cases}$$

according to Hernquist (1990).

Table B1. Full set of gravitational lenses used for this analysis.

Lens	z_L	$\sigma_{\rm obs}$ (km s^{-1})	$\sigma_{\rm lens}$ (km s^{-1})	$R_{\rm eff}$ (kpc)	$R_{\rm lens}$ (kpc)	$M_{\rm lens}$ ($10^{11} \times {\rm M}_\odot$)	$M_{\rm vir}$ ($10^{11} \times {\rm M}_\odot$)	L_I ($10^{11} \times {\rm L}_\odot$)	$M_{\rm lens}/L_I$ (${\rm M}_\odot/{\rm L}_\odot$)	Reference
B0047−2808	0.4850	229 ± 15	189.0 ± 6.4	5.324	7.440	2.084 ± 0.141	3.059 ± 0.401	0.760	2.74	*a b a*
CFRS03.1077	0.9380	256 ± 19	306.6 ± 22.0	–	15.905	–	–	–	–	*a c a*
Q0957 (2D)	0.3600	288 ± 9	$351.6^{+12.8}_{-10.4}$	22.64	25.529	$30.458^{+2.477}_{-1.583}$	20.58 ± 1.29	4.922	6.19	*a d j*
PG1115+080	0.3100	281 ± 25	190.8 ± 8.4	2.072	6.188	0.826 ± 0.073	1.792 ± 0.319	0.671	1.23	*a e a*
HST14176	0.8100	230 ± 14	245.6 ± 4.0	5.190	12.780	3.430 ± 0.112	3.008 ± 0.366	3.910	0.88	*a f a*
HST15433	0.4970	108 ± 14	156.2 ± 2.8	–	4.601	–	–	–	–	*a c a*
B1608+656	0.6300	247 ± 35	242.6 ± 18.4	4.291	15.542	2.766 ± 0.420	2.868 ± 0.813	3.354	0.82	*a g a*
MG2016+112	1.0100	304 ± 27	330.4 ± 29.6	1.707	19.388	2.041 ± 0.366	1.729 ± 0.307	2.128	0.96	*a h a*
Q2237+030	0.0400	215 ± 30	146.4 ± 2.8	2.993	0.743	0.703 ± 0.027	1.516 ± 0.423	0.542	1.30	*a i a*
J0037−094	0.1954	265 ± 10	$230.4^{+33.6}_{-36.0}$	6.804	6.470	$3.956^{+1.239}_{-1.139}$	5.234 ± 0.395	1.990	1.99	*a*
J0737+321	0.3223	310 ± 15	233.6 ± 6.4	9.823	5.333	5.874 ± 0.322	10.34 ± 1.00	3.544	1.66	*a*
J0912+002	0.1642	313 ± 12	$276.0^{+11.2}_{-15.2}$	9.203	5.271	$7.679^{+0.637}_{-0.821}$	9.877 ± 0.757	2.289	3.35	*a*
J0956+510	0.2405	299 ± 16	$266.8^{+7.6}_{-8.4}$	8.607	6.201	$6.710^{+0.390}_{-0.414}$	8.430 ± 0.902	2.572	2.61	*a*
J1205+491	0.2150	235 ± 10	$230.2^{+10.6}_{-8.6}$	7.805	5.138	$4.531^{+0.427}_{-0.332}$	4.722 ± 0.402	1.936	2.34	*a*
J1330−014	0.0808	178 ± 9	$142.3^{+20.9}_{-20.7}$	1.244	1.696	$0.276^{+0.087}_{-0.074}$	0.432 ± 0.044	0.147	1.88	*a*
J1636+470	0.2282	221 ± 15	$230.7^{+9.3}_{-12.3}$	5.256	6.150	$3.065^{+0.252}_{-0.318}$	2.812 ± 0.382	1.376	2.23	*a*
J2300+002	0.2285	283 ± 18	$239.8^{+10.6}_{-7.8}$	6.256	5.278	$3.942^{+0.355}_{-0.253}$	5.489 ± 0.698	1.522	2.59	*a*
J2303+142	0.1553	260 ± 15	$242.7^{+14.9}_{-17.9}$	7.901	5.303	$5.098^{+0.646}_{-0.724}$	5.851 ± 0.675	2.333	2.19	*a*
ACO 1689	0.1830	1400 ± 300	$1188.7^{+40.0}_{-56.0}$	400.0	237.6	6192^{+424}_{-570}	8589 ± 2187	33.48	185	*b*
ACO 2667	0.2330	960^{+190}_{-120}	$762.0^{+7.2}_{-8.0}$	–	98.01	–	–	–	–	*c*

Note. The first nine lenses are from CASTLES, the following nine from SLACS and the last two are clusters. The image positions and flux data have been taken from *HST* data (http://www.cfa.harvard.edu/glensdata/), Bolton et al. (2006) and Covone et al. (2006). The symbols mark the references for the data in the columns z_L, $\sigma_{\rm obs}$ and $R_{\rm eff}$, and refer to the following publications: [a](Rusin et al. 2003b), [b](Koopmans & Treu 2003), [c](Treu & Koopmans 2004), [d](Tonry & Franx 1999), [e](Tonry 1998), [f](Ohyama et al. 2002), [g](Koopmans et al. 2003), [h](Koopmans & Treu 2002), [i](Foltz et al. 1992), [j](Keeton, Kochanek & Falco 1998), [k](Bolton et al. 2006), [l](Łokas et al. 2006) and [m](Covone et al. 2006). Note that $\sigma_{\rm obs}$ is the kinematic central velocity dispersion, which is in the case of SLACS lenses the line-of-sight stellar velocity dispersion measured by the 3 arcsec diameter SDSS spectroscopic fibre. The $\sigma_{\rm lens}$ values are determined for the projected distance $R_{\rm lens}$ from the outermost lensing image to the central lensing mass. The effective radii given in arcsec in Rusin et al. (2003b) and Bolton et al. (2006) have been transformed into kpc. All quantities in the table assume $H_0 = 72$ km s^{-1} Mpc^{-1}, $\Omega_{\rm m} = 0.3$ and $\Omega_\Lambda = 0.7$.

Table B2. List of previously found FP parameters and the results of this paper.

Reference	a	b
(Dressler et al. 1987)	1.33 ± 0.05	-0.83 ± 0.03
(Djorgovski & Davis 1987)	1.39 ± 0.14	-0.90 ± 0.09
(Lucey et al. 1991)	1.27 ± 0.07	-0.78 ± 0.09
(Guzman et al. 1993)	1.14	−0.79
(Jørgensen et al. 1996)	1.24 ± 0.07	-0.82 ± 0.02
(Hudson et al. 1997)	1.38 ± 0.04	-0.82 ± 0.03
(Scodeggio et al. 1997)	1.25 ± 0.02	-0.79 ± 0.03
(Pahre et al. 1998)	1.53 ± 0.08	-0.79 ± 0.03
(Müller et al. 1998)	1.25	−0.87
(Gibbons et al. 2000)	1.39 ± 0.04	-0.84 ± 0.01
(Colless et al. 2001)	1.22 ± 0.09	-0.84 ± 0.03
(Bernardi et al. 2003)	1.49 ± 0.05	-0.75 ± 0.01
This paper		
For $\sigma_{\rm lens}$	1.08	−0.77
(upper limit)	1.28	−0.82
(lower limit)	0.90	−0.72
For $\sigma_{\rm obs}$	1.33	−0.83
(upper limit)	1.64	−0.91
(lower limit)	1.08	−0.77

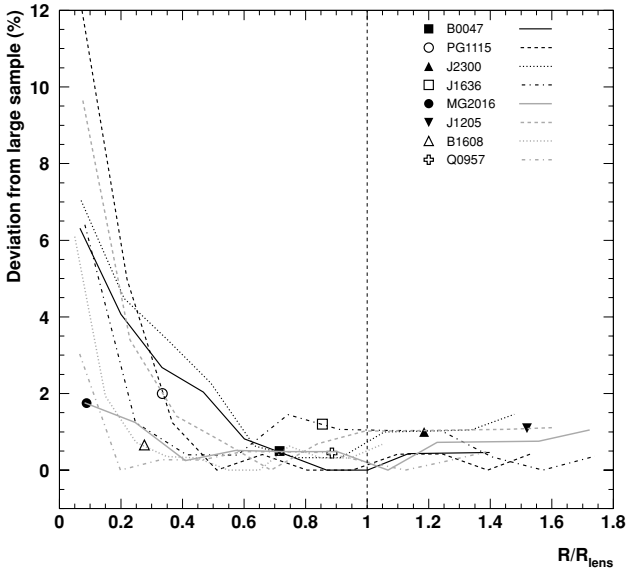

Figure B1. Absolute deviation of formal velocity dispersion curve of a small ensemble from the one of a large ensemble in terms of per cent plotted against the radius in terms of $R_{\rm lens}$. The dashed vertical line denotes $R_{\rm lens}$. The listed markers indicate the deviation of $\sigma_{\rm lens}$ at the effective radius.

APPENDIX B:

In Fig. B1, the absolute deviation between the average formal velocity dispersion of an ensemble of 100 models and one with about 10 000 models, which we take as close to exact representation of the lens model, is shown in terms of percentage. The analysis is done for a subsample of doubles, quads and multiple object systems of SLACS and CASTLES lenses. We find that $\sigma_{\rm lens}(R_{\rm lens})$ $[\sigma_{\rm lens}(R_{\rm eff})]$ of the smaller ensemble deviates less than $\sim$1 per cent ($\sim$2 per cent) from the corresponding velocity dispersion for a larger ensemble.

Figs B2, B3 and B4 (in the online version of this paper only – see Supporting Information) show, respectively, the CASTLES lenses, SLACS lenses and lensing clusters used in this analysis.

SUPPORTING INFORMATION

Additional Supporting Information may be found in the online version of this article:

Figure B2. CASTLES lenses used in this analysis.
Figure B3. SLACS lenses used in this analysis.
Figure B4. Lensing clusters used in this analysis.

Please note: Wiley-Blackwell are not responsible for the content or functionality of any supporting materials supplied by the authors. Any queries (other than missing material) should be directed to the corresponding author for the article.

This paper has been typeset from a TEX/LATEX file prepared by the author.